

# UV continuum emission and diagnostics of hydrogen-containing non-equilibrium plasmas

Boris P. Lavrov and Alexei S. Melnikov

*Faculty of Physics, St.-Petersburg State University, 198904, Russian Federation*

Marko Käning and Jürgen Röpcke

*Institute for Low Temperature Plasma Physics, 17489 Greifswald, Federal Republic of Germany*

(May 18, 2019)

## Abstract

For the first time the emission of the radiative dissociation continuum of the hydrogen molecule ( $a^3\Sigma_g^+ \rightarrow b^3\Sigma_u^+$  electronic transition) has been used as a source of information for the spectroscopic diagnostics of non-equilibrium plasmas. It is shown that in the wavelength range  $\lambda = 220 - 400$  nm the shape of the continuum is sensitive to the ground  $X^1\Sigma_g^+$  state vibrational temperature for  $T_{\text{vib}} = 2000 \div 8000$  K. The absolute intensity of the continuum is proposed to be used for an estimation of the rate of the electron impact dissociation  $(d[H_2]/dt)_{\text{diss}}$ . General considerations are illustrated with examples of experiments in capillary-arc and microwave discharges. It was observed in the H<sub>2</sub>+Ar plasma that the shape of the continuum depends on the ratio of the mixture components. Absorption measurements of the population of the 3s<sup>2</sup>3p<sup>5</sup>4s levels of Ar I together with certain computer simulations confirmed that the Ar\* $\rightarrow$ H<sub>2</sub> excitation transfer should be taken into account. In our conditions (power flux near microwave applicator windows: 4 W cm<sup>-2</sup>, pressure  $p = 0.5$  mbar) the following values were obtained for the microwave discharge:  $T_{\text{vib}} \lesssim 3000$  K,  $(d[H_2]/dt)_{\text{diss}} \approx 10^{17}$  cm<sup>-3</sup> s<sup>-1</sup>, typical contributions of the excitation transfer were 10-30% of the total population of the  $a^3\Sigma_g^+$  state.

52.70.-m, 52.70.Kz, 52.20.Fs, 52.20.Hv

## I. INTRODUCTION

Experimental and theoretical studies of the emission of the  $H_2$  radiative dissociation continuum ( $a^3\Sigma_g^+ \rightarrow b^3\Sigma_u^+$  electronic transition) have a long and interesting history. They were stimulated by molecular spectroscopy and quantum chemistry [1–7], investigations of hydrogen containing plasmas [8–10] and astrophysics [11,12]. Since the first work of Houtermans [13] the  $a^3\Sigma_g^+ \rightarrow b^3\Sigma_u^+$  transition has been studied as a possible laser system (see [14–17] and Refs. herein). It is widely used in UV and VUV light sources [8,18–21].

Various radiative and collisional elementary processes related to the phenomenon were studied in numerous works (see below). At first the kinetics of excitation-deactivation of  $a^3\Sigma_g^+, v'$  vibronic states of  $H_2$  and  $D_2$  in plasma were studied on the basis of measurements of relative continuum intensities, electron energy distribution function  $F(\varepsilon)$  (by Langmuir probes), and gas temperature in hollow cathode and capillary-arc discharges [9]. Simple systems of the excitation-deactivation balance equations were used for the explanation of well-known empiric phenomena: 1) the independence of the shape of the continuum on discharge conditions, and 2) the difference between spectral distributions in  $H_2$  and  $D_2$  continua. This approach was later improved to be able to consider the continuum intensity in an absolute scale [10]. It was found that the knowledge of radiative and collisional transition probabilities together with accurate measurements of  $F(\varepsilon)$  makes it possible to calculate the intensities in hydrogen low-pressure plasma with an accuracy of 20–30%, which is acceptable for practical purposes. As far as we know, the  $H_2$  continuum emission was never used or proposed to be used for a determination of plasma parameters, i. e., for spectroscopic plasma diagnostics.

The experimental data contain two different sources of information: the relative spectral distribution and the total absolute intensity of the continuum. In the absence of self-absorption the first one is directly connected with the population density distribution over vibrational levels of the  $a^3\Sigma_g^+$  state. In low pressure plasmas the levels are populated predominantly by direct electron impact excitation and the deactivation is mainly due to spontaneous emission. In this case the relation between the vibrational population density distributions in excited and ground electronic states may be obtained within corona-like models [9]. So the shape of the continuum may be used for a determination of the vibrational density distribution of the ground state of  $H_2$  in non-equilibrium plasmas.

On the other hand every act of the continuum emission leads to a dissociation of a hydrogen molecule. Therefore, an absolute value of the continuum intensity is in principle connected with the rate of radiative dissociation via the  $a^3\Sigma_g^+$  state and also may be used for an estimation of the rate of electron impact dissociation. The main goal of this paper is to investigate both opportunities and to check them experimentally. Some preliminary results were already reported in [22].

## II. INTENSITIES OF $H_2$ BANDS AND VIBRATIONAL TEMPERATURE

The dissociation continuum of the hydrogen molecule is caused by spontaneous transitions from the upper bound  $a^3\Sigma_g^+$  electronic state to the lower  $b^3\Sigma_u^+$  repulsive state. The spectral distribution  $I_{ab}(\lambda)$  of the continuum intensity (number of quanta emitted within

unit range of wavelengths per unit volume and per second) is related to the population densities  $N_{av'}$  of the excited  $a^3\Sigma_g^+, v'$  vibronic levels, as

$$I_{ab}(\lambda) = \sum_{v'} N_{av'} \cdot A_b^{av'}(\lambda), \quad (1)$$

where  $v'$  – vibrational quantum number,

$$N_{av'} = \sum_{N'} N_{av'N'}, \quad (2)$$

the total population density of the upper vibronic state,  $N_{av'N'}$  – populations of  $a^3\Sigma_g^+, v', N'$  electronic-vibro-rotational levels (their very small triplet splitting may be neglected),  $N'$  – rotational quantum number of the total angular momentum excluding electron spin, and  $A_b^{av'}(\lambda)$  – spectral distribution of the spontaneous emission transition probability (Einstein coefficients for various wavelengths of  $a^3\Sigma_g^+, v' \rightarrow b^3\Sigma_u^+$  transitions). We have neglected the rather small effect of vibro-rotation interaction and assume the transition probabilities being independent on  $N'$ .

For  $H_2$  molecules the values of  $A_b^{av'}(\lambda)$  should be considered as well-known nowadays because they have been calculated in several works [1,5–7,14] and checked experimentally [4], being in rather good agreement [7]. We used the results of [6,7] shown in Table I. These are the only data presented in table form suitable for applications. In Fig. 1 the data are visualized for the transitions from  $a^3\Sigma_g^+, v'=0-3$  levels for  $\lambda = 200 - 450$  nm. The probability of transitions from various vibronic levels has maxima in different wavelength regions due to oscillations of the vibrational wave functions of the upper state. So the spectral distribution of the continuum intensity  $I_{ab}(\lambda)$  has a certain informational content about the population density distribution over vibrational levels of the  $a^3\Sigma_g^+$  electronic state. In principle, measurements of the intensity  $I_{ab}(\lambda)$  may be used for the determination of the populations  $N_{av'}$  in relative or even in absolute scale by Eq. (1).

It should be noted that even this very first stage of the data processing belongs to the class of so-called reverse (or inversion) problems, which are known to be not well posed (sometimes they are called “ill-posed”). The final result – a certain set of the populations  $N_{av'}$  – depends (in principle) not only on the values of the actual populations in the plasma, but may be influenced by so-called *a priori* information: the number of adjusted parameters ( $N_{av'}$ ), the number of experimental data points, the experimental errors and the algorithm used.

In the present work we used for the solution of this and other reverse problems the least-square fitting, i. e., the minimization of the functional

$$\chi^2 = \frac{1}{l-m} \sum_{i=1}^l \left( \frac{Y_i^{\text{calc}}(a_1, \dots, a_m) - Y_i^{\text{expt}}}{\sigma_i} \right)^2 \quad (3)$$

in the multidimensional space of parameters  $a_1, \dots, a_m$  used in a theoretical model. Here  $Y_i^{\text{calc}}(a_1, \dots, a_m)$ ,  $Y_i^{\text{expt}}$  – calculated and experimental data,  $l$  – total number of data points,  $m$  – number of adjusted parameters,  $\sigma_i$  – standard deviations of the experimental data. The standard deviations of optimal values of the adjusted parameters may be estimated as square roots of diagonal terms of the covariance matrix [23].

We used a minimization algorithm analogous to a linear regression [23] with the following substitutions:  $Y_i^{\text{expt}} \equiv I_{ab}^{\text{expt}}(\lambda_i)$  from experiment,  $Y_i^{\text{calc}} \equiv I_{ab}(\lambda_i)$  from Eq. (1),  $\sigma_i \equiv 0.07 \cdot I_{ab}^{\text{expt}}(\lambda_i)$  corresponding to 7% random experimental error of the measurement,  $m \equiv v'_{\max} + 1$ ,  $\lambda_i$  was varied in the range 220 – 400 nm. Experimental errors were estimated by averaging of several measurements for the same conditions of the plasma. They are mainly caused by random noise, non-sufficient stability of the discharges during the experiments and restricted reproducibility. The value of  $v'_{\max}$  had to be adjusted in such a way that reliable results can be obtained from the minimization procedure. The values of  $A_b^{av'}(\lambda)$  were interpolated by cubic splines from Table I.

Values of  $N_{av'}$  may be sometimes interesting themselves (see the examples below). But on the other hand, in non-equilibrium plasmas the rovibronic level populations in excited electronic states are connected with those in the ground electronic state [24]. Under certain conditions they may be used for the spectroscopic determination of vibrational [9,25] and rotational temperatures [26–28]. In the present work we were able to measure also the populations  $N_{dv'N'}$  of the  $d^3\Pi_u^-$ ,  $v'=0-5, N'=1-5$  rovibronic levels by the Q-branch lines of the Fulcher- $\alpha$  bands. For further analysis let us consider the excitation-deactivation balance equation for the electronically excited  $n', v', N'$  rovibronic level which may be written as

$$\sum_{vN} N_{XvN} \cdot n_e \cdot \alpha_{XvN}^{n'v'N'} + I_{n'v'N'}(\alpha, \beta, \gamma, \dots) = N_{n'v'N'} \left( \frac{1}{\tau_{n'v'N'}^{\text{rad}}} + \frac{1}{\tau_{n'v'N'}^{\text{coll}}} \right), \quad (4)$$

where  $I_{n'v'N'}(\alpha, \beta, \gamma, \dots)$  – the rate of secondary excitation processes (cascades, recombination and so forth);  $\tau_{n'v'N'}^{\text{rad}}$  – radiative lifetime of the  $n'v'N'$  level;  $\tau_{n'v'N'}^{\text{coll}}$  – effective lifetime describing the decay of the  $n'v'N'$  level due to quenching in collisions of the excited molecule with electrons, atoms and unexcited molecules. The rate coefficient of direct electron impact excitation

$$\alpha_{XvN}^{n'v'N'} = \langle \sigma \mathbf{v} \rangle_{XvN}^{n'v'N'} = \int_{\varepsilon_{th}}^{\infty} \sqrt{\frac{2\varepsilon}{m}} \sigma_{XvN}^{n'v'N'}(\varepsilon) F(\varepsilon) d\varepsilon, \quad (5)$$

where  $\sigma_{XvN}^{n'v'N'}(\varepsilon)$  – corresponding cross section;  $\mathbf{v}, \varepsilon$  – velocity and corresponding energy of the incident electron;  $\varepsilon_{th}$  – threshold energy of  $n', v', N' \leftarrow X, v, N$  transition;  $F(\varepsilon)$  – the electron energy distribution function.

For plasma diagnostics the most simple limit case (often called corona or corona-like model) is that of low-pressure plasmas with small input power. Under such conditions the levels are predominantly excited by direct electron impact excitation and their decay is mainly due to spontaneous emission. An additional population of the  $a^3\Sigma_g^+$  state due to cascades from  $e^3\Sigma_g^+$  and  $d^3\Pi_u^-$  states was taken into account in [10] and found to be less than 20%. The radiative and collisional quenching lifetimes are estimated to be equal at 3 mbar for  $a^3\Sigma_g^+$  and at 0.75 mbar for  $d^3\Pi_u^-$  states (see [10,29]).

It may be seen from Eqs. (2) and (3) that even in the most favorable case for plasma diagnostics the populations  $N_{n'v'N'}$  depend not only on the distribution  $N_{XvN}$ . Radiative transition probabilities, lifetimes and electron impact cross sections for single rovibronic levels and transitions should be known as well as the electron energy distribution function. Moreover the determination of  $N_{XvN}$  from measured  $N_{n'v'N'}$  and certain system of equations (2) for various  $v'$  and  $N'$  lead to a reverse problem.

The transition probabilities for  $d^3\Pi_u^-, v', N'=1 \rightarrow a^3\Sigma_g^+, v'', N''=1$  transitions [Q1 lines of Fulcher- $\alpha$  bands ( $d^3\Pi_u^- \rightarrow a^3\Sigma_g^+$  electronic transition)] were obtained semiempirically in the framework of the adiabatic approximation from experimental data about wave numbers, branching ratios in  $v''$ -progressions and radiative lifetimes [30]. The results for the first seven diagonal ( $v'=v''=v$ ) bands are presented in Table II together with semiempirically predicted [30] and experimental values of radiative lifetimes [28,29].

One may see a noticeable discrepancy between semiempirical and experimental lifetimes of  $d^3\Pi_u^-, v'=4-6, N'=1$  rovibronic levels due to non-adiabatic effects neglected in the adiabatic approximation (see also [10,29]). Therefore, only the first four diagonal bands may be used for the determination of  $T_{\text{vib}}$ . On the other hand this effect did not influence the values of the rotational temperatures derived from the populations of  $d^3\Pi_u^-, v' > 3$  levels in [28]. It may be considered as an indication, that the rate of the additional decay, associated with a non-adiabatic coupling of the vibronic levels lying above the  $\text{H}(n=1) + \text{H}(n=2)$  dissociation limit, is almost independent on  $N'$  (here  $n$  is the principle quantum number). It seems quite reasonable, if the perturbation is due to an electron-rotational interaction with a continuum (the hypothesis proposed in [31]). Because of the lack of information about  $N'$ -dependences of the transition probabilities and the lifetimes they are considered as independent on the rotational quantum number in accordance with an adiabatic approximation.

The radiative lifetimes of  $a^3\Sigma_g^+, v'$  vibronic states of  $\text{H}_2$  have been studied in numerous works both experimentally [2,3,12,32–34] and by *ab initio* calculations [1,5]. All available data are collected in Table III. One may see, that: (1) Nothing is known about  $N'$ -dependences of the lifetimes, so we have to assume independence on  $N'$ . (2) Experimental data are obtained only for low vibronic states. (3) The experimental and calculated data are in very good accordance for  $v'=0-2$ , but for higher  $v'$  only *ab initio* data are available.

To be in consistence with the transition probabilities listed in, Table I, we used values of  $\tau_{av'}$  marked in Table III as “p.w.”. The lifetimes for  $v'=0-2$  were obtained by integration of the tabulated values of probability. The values labeled with an asterisk for  $v'=3-6$  were obtained by extrapolating the lifetimes with the help of a third order polynomial fit of the data from [5] and a constant factor obtained from the average value of the ratios with our values for  $\tau_{av'}$  and  $v'=0-2$ . This was necessary because for  $v' > 2$  one can see in Table I that some quantity of transition probability resides below the lower table margin of  $\lambda = 160$  nm. Therefore, the calculation of the  $\tau_{av'}$  from the tabulated  $A_b^{av'}(\lambda)$  values leads to an overestimation of the lifetimes.

The dependences of  $d^3\Pi_u^-, v', N' \leftarrow X^1\Sigma_g^+, 0, N$  electron impact excitation on incident electron energy have been studied in [35–37]. For singlet-triplet transitions they have normal form: a sharp increase from the threshold to the maximum and a rather sharp decrease for higher energies. The data of [35,37] are in good accordance and they were used for the extraction of the cross sections for different  $v'$  from measured rate coefficients and  $F(\varepsilon)$  in [9]. The relative cross sections  $\sigma_{X01}^{dv'1}/\sigma_{X01}^{d21}$  in maximum are shown in Table IV together with corresponding ratios of the Franck-Condon factors calculated in [38]. One may see noticeable deviation of measured values from those calculated in the Franck-Condon approximation. This discrepancy was interpreted as an evidence of a remarkable dependence of the scattering amplitude on the internuclear distance (non-Franck-Condon effect). The data from [9] have been used for the determination of the complete set of the cross sections for various  $v, v'$  and  $N, N'$  [39].

It is important to take into account that the relative cross sections in [9] are based on radiative transition probabilities and lifetimes obtained in adiabatic approximation (almost the same as in Table IV). As we already mentioned above the lifetimes of  $v'=4-6$  are in contradiction with such extrapolation. New data about  $\tau_{dv'1}$  [29] and  $A_{av''1}^{dv'1}$  [30] should be used for the determination of the cross sections from the line intensities measured in [9]. We made the recalculation and got the data presented in the sixth column of Table IV. One may see that they are in rather good agreement with corresponding ratios of Franck-Condon factors. It means that the dependence of the scattering amplitude on the internuclear distance is negligible in the case of the  $d^3\Pi_u^- \leftarrow X^1\Sigma_g^+$  electron impact excitation of  $\text{H}_2$ . This was recently confirmed by *ab initio* calculations [40].

Nothing is known, so far as we know, about the cross sections for the  $a^3\Sigma_g^+, v', N' \leftarrow X^1\Sigma_g^+, v, N$  excitation. Therefore, for both  $d^3\Pi_u^- \leftarrow X^1\Sigma_g^+$  and  $a^3\Sigma_g^+ \leftarrow X^1\Sigma_g^+$  transitions we assume that the rate coefficients of electron impact excitation only for  $N' = N$  rovibronic transitions has non-zero values. They are independent on  $N$  and proportional to corresponding Franck-Condon factors, i. e.,

$$\alpha_{XvN}^{n'v'N'} \approx \alpha_{Xv}^{n'v'} \propto Q_{Xv}^{n'v'}, \quad \text{when} \quad \Delta N' \equiv N' - N = 0 \quad (6)$$

$$\text{and} \quad \alpha_{XvN}^{n'v'N'} = 0 \quad \text{for} \quad \Delta N' \neq 0 \quad (7)$$

thus neglecting the momentum transfer in electron impact excitation [37,41] and the rather small dependence of  $\alpha$  on  $F(\varepsilon)$ . Most accurate values of Franck-Condon factors for  $d^3\Pi_u^- \leftarrow X^1\Sigma_g^+$  and  $a^3\Sigma_g^+ \leftarrow X^1\Sigma_g^+$  transitions were calculated in [38]. The data are presented in Tables V and VI.

Vibrational and rotational energies are not well separated in the ground electronic state of  $\text{H}_2$  because of the small mass of the nuclei. Just to have a certain ability to characterize the distributions over the vibrational levels we may introduce the vibrational temperature by

$$N_{Xv} = \sum_N N_{XvN} = \sum_N \frac{[\text{H}_2] \cdot \exp\left(-\frac{\Delta E_{Xv}}{kT_{\text{vib}}}\right) \cdot (2N+1) \cdot \exp\left(-\frac{\Delta E_{XvN}}{kT}\right)}{\sum_v \exp\left(-\frac{\Delta E_{Xv}}{kT_{\text{vib}}}\right) \sum_N (2N+1) \cdot \exp\left(-\frac{\Delta E_{XvN}}{kT}\right)} = [\text{H}_2] \cdot \frac{\exp\left(-\frac{\Delta E_{Xv}}{kT_{\text{vib}}}\right)}{\mathcal{P}(T_{\text{vib}})}, \quad (8)$$

where  $[\text{H}_2]$  – total concentration of molecules,  $\Delta E_{Xv} = E_{Xv0} - E_{X00}$ ,  $\Delta E_{XvN} = E_{XvN} - E_{Xv0}$  – vibrational and rotational energy differences,  $T_{\text{vib}}$  and  $T$  – vibrational and translational temperatures,  $\mathcal{P}(T_{\text{vib}})$  – the vibrational partition function. So we assume that in all vibrational levels of the  $X^1\Sigma_g^+$  state the populations of the rotational levels are in Boltzmann equilibrium with the gas temperature  $T$ .

Taking into account all the assumptions discussed above, the balance equation (4) may be written for the populations of  $d^3\Pi_u^-, v'$  vibronic states after summation over rotational levels in the following form

$$\frac{1}{\mathcal{P}(T_{\text{vib}})} \sum_v Q_{Xv}^{dv'} \cdot \exp\left(-\frac{\Delta E_{Xv}}{kT_{\text{vib}}}\right) \propto \frac{N_{dv'}}{\tau_{dv'}}. \quad (9)$$

For the determination of  $T_{\text{vib}}$  we solved numerically the system of equations (9) for various  $v'$  with experimental data about  $N_{dv'}$  derived from the intensities of the Fulcher- $\alpha$  Q-branch lines:

$$N_{dv'} = \sum_N \frac{I_{avN}^{dvN}}{A_{avN}^{dvN}}. \quad (10)$$

In the framework of our model the continuum intensity can be written as

$$I_{ab}(\lambda, T_{\text{vib}}) \propto \frac{1}{\mathcal{P}(T_{\text{vib}})} \sum_{v'} A_b^{av'}(\lambda) \cdot \tau_{av'} \cdot \sum_{v=0}^{v'_{\max}} Q_{Xv}^{av'} \cdot \exp\left(-\frac{\Delta E_{Xv}}{kT_{\text{vib}}}\right). \quad (11)$$

To be able to work with relative intensities we may introduce the normalized relative intensity

$$J_{ab}(\lambda, \lambda_0, T_{\text{vib}}) = I_{ab}(\lambda, T_{\text{vib}}) / I_{ab}(\lambda_0, T_{\text{vib}}), \quad (12)$$

which is equal to unity for  $\lambda = \lambda_0$ .

The normalized intensities (12) may be tabulated for various values of  $T_{\text{vib}}$  and then may be used for a determination of the vibrational temperature by least squares fitting (3) of experimental and calculated continuum intensity distributions.

When the vibrational temperature is sufficiently low and

$$Q_{X0}^{av'} \gg \sum_{v=1} Q_{Xv}^{av'} \cdot e^{-\frac{\Delta E_{Xv}}{kT_{\text{vib}}}}, \quad (13)$$

then the excitation from vibronic levels with  $v > 0$  may be neglected and

$$J_{ab}(\lambda, \lambda_0, 0) = \frac{\sum_{v'=0}^{v'_{\max}} A_b^{av'}(\lambda) \cdot \tau_{av'} \cdot Q_{X0}^{av'}}{\sum_{v'=0}^{v'_{\max}} A_b^{av'}(\lambda_0) \cdot \tau_{av'} \cdot Q_{X0}^{av'}} \quad (14)$$

represents the shape of the continuum for  $T_{\text{vib}} \rightarrow 0$ . It does not depend on discharge conditions [9] and may be easily calculated because molecular constants in Eq. (14) are known. The results of such calculation for  $\lambda_0 = 400$  nm and  $v'_{\max} = 6$  are presented in the last column of Table I.

The ratio

$$J'_{ab}(\lambda, \lambda_0, T_{\text{vib}}) = J_{ab}(\lambda, \lambda_0, T_{\text{vib}}) / J_{ab}(\lambda, \lambda_0, 0) \quad (15)$$

may also be calculated for various values of the vibrational temperature and then be used as a nomogram for the determination of  $T_{\text{vib}}$  from measured relative continuum intensity without solving the inverse problem by a minimization of Eq. (3). The results of such calculations for a limited number of  $T_{\text{vib}} = 2000 - 8000$  K are shown in Fig. 2. One may see that the ratio (15) has some sensitivity to the vibrational temperature especially near 300 nm. For this particular wavelength we may organize a graph of  $J'_{ab}(\lambda = 300 \text{ nm}, \lambda_0 = 400 \text{ nm}, T_{\text{vib}})$  versus  $T_{\text{vib}}$  presented in Fig. 3 where the sensitivity is even more clear. This dependence may be used as a nomogram too, being especially useful for *in situ* control of plasmachemical processes.

### III. MEASUREMENTS

#### A. Experimental setup

The experiments in pure hydrogen and  $H_2+Ar$  plasmas were carried out in two different gas discharges.

The first one (USSR standard spectral lamp DVS-25) is a hot cathode arc with 2 mm diameter constriction analogous to those used in [19,20]. The discharge device was filled with 8 mbar of spectrally pure hydrogen. The range of the discharge current  $I = 10 - 300$  mA allowed us to achieve rather high current densities  $j = 0.3 - 9.6$  A/cm<sup>2</sup>.

The second plasma source was a  $H_2+Ar$  microwave discharge excited by a planar microwave applicator similar to that described in [42]. The inner dimensions of the discharge vessel are  $15 \times 21 \times 120$  cm<sup>3</sup> and the area of the quartz microwave windows was  $8 \times 40$  cm<sup>2</sup>. The microwave power was fed in by a generator (SAIREM, GMP 12 KE/D, 2.45 GHz). We were able to measure the total input ( $W$ ) and reflected power, the latter was in our conditions ( $W = 1.5$  kW) always negligible (< 4%). The input power flux in the plane of the applicator windows was roughly estimated to about 4 W/cm<sup>2</sup> assuming 20% heat loss to coolant and environment. Gas flow controllers and a butterfly valve in the gas exhaust allow to have an independent control of gas inflow ( $\varphi = 100$  sccm) and pressure ( $p = 0.5-5$  mbar). The purity of gases was 99.996%.

The central part of the plasma along the axis of the capillary discharge was focused by a quartz achromatic lens onto the entrance slit of a monochromator. In the microwave plasma the line of sight was 12 mm below the microwave windows of the applicator. For measurements of the continuum intensity we used a 0.5 m Czerny-Turner monochromator (Acton Research Corporation Spectra Pro-500) with a grating of 600 grooves per mm in the first order. The line intensities however were measured using a high resolution 1 m double monochromator of Czerny-Turner type with 1800 grooves per mm (Jobin Yvon RAMANOR U1000) in the first order. The output light was detected by a CCD matrix detector (TE-cooled, 512×512 pixel, size of image zone:  $9.7 \times 9.7$  mm<sup>2</sup>) of the Optical Multichannel Analyzer PARC OMA IV connected with a 40 MHz 486DX computer.

The wavelength calibration was done by means of known Ar lines observed in the  $H_2+Ar$  microwave plasma. Special software made it possible to collect and analyze the recorded spectra.

The relative spectral sensitivity of the spectroscopic system in the range  $\lambda = 200 - 450$  nm has been obtained using a deuterium lamp (Heraeus Noble Light DO651MJ) calibrated by the Physikalisch-Technische Bundesanstalt (Braunschweig). The absolute value of the sensitivity for  $\lambda = 350$  nm was determined with a tungsten ribbon lamp. Its current-temperature calibration has been performed by the Russian State Institute of Standards (St.-Petersburg). We used two different currents corresponding to the absolute temperatures of tungsten  $T = 2637$  and  $2763$  K. This gave us usually a spread in the values of the sensitivity (at  $\lambda = 350$  nm) of less than 1%. The emissivity coefficient of the tungsten ribbon for these temperatures was taken from [43] and used for the calculation of the spectral distribution of emission intensity.

Some typical experimental records of the spectra of a standard deuterium lamp (a), pure hydrogen capillary-arc discharge (b) and a  $H_2+Ar$  plasma of the microwave discharge (c)

are presented in Fig. 4. The non-monotonic structure in the range  $\lambda = 250 - 350$  nm is connected with the spectral distribution of the sensitivity. In the long-wavelength end of the first two records the band (actually multiline) spectra of  $D_2$  and  $H_2$  molecules may be seen. One may see also that in spite of the gas flow mode our microwave plasma is not spectrally pure. It contains some impurities: oxygen (283 nm), OH-radical (bands at 283, 310 – 320 nm), NH-radical (336 nm) and  $N_2$  molecule (bands of the 2nd positive system 280 – 400 nm mixed with  $H_2$  bands). It should be noted that some lines are overexposed in the record shown in Fig. 4(c). The data of the continuum intensity were manually extracted from the measured intensity distribution.

## B. Pure hydrogen DC capillary-arc discharge

The relative continuum intensity and Q-branch lines of Fulcher- $\alpha$  bands were measured in the current range mentioned above. The shape of the continuum was observed to be independent on the current within the experimental errors. A typical result used in further analysis is presented in Fig. 5. The low wavelength margin is limited by a sharp decrease of the sensitivity of our spectrometrical system.

To find the optimum number of adjusted parameters we made a  $\chi^2$  minimization [Eq. (3)] with various  $m = (v'_{\max} + 1)$ . The results of the calculations, made for the experimental data of Fig. 5, are presented in Table VII.  $\chi^2$  shows a monotonic decrease and becomes lower than unity for  $v'_{\max} \geq 3$ . Another characteristic, presented in the table, is

$$\rho_{\max} = \max(\rho_i) \quad \text{with} \quad \rho_i = \sqrt{1 - 1/\Phi_i}, \quad (16)$$

$$\text{where} \quad \Phi_i = Z_{ii}Z_{ii}^{-1} \quad \text{and} \quad Z_{lk} = \frac{\partial^2(\chi^2)}{\partial a_l \partial a_k}. \quad (17)$$

The magnitudes  $\rho_i$  are characteristics of the precision of the solution. Its zero value corresponds to the limit case of total independence of the parameters, while  $\rho_i=1$  means that the parameter  $a_i$  may be expressed as a linear combination of the other parameters and therefore the number of adjusted parameters should be decreased. It may be seen from Table VII that in our case  $\rho_{\max}$  is growing with the increase of  $m$ ;  $\rho_{\max}$  is near to 1 for  $v'_{\max} > 3$ .

The maximum value of the relative standard deviation of the parameters  $(\Delta N_{av'}/N_{av'})_{\max}$  (in our case usually observed for  $v'=v'_{\max}$ ) is small and almost independent on  $v'_{\max}$  for  $v'_{\max}=0-3$ , then it jumps to about 0.83 at  $v'=4$  and becomes much bigger for  $v'=5,6$ . It means that the standard deviation of  $N_{av}$  derived from our spectrum is almost the same as its optimal value.

Taking into consideration the results of Table VII we came to the conclusion that in our case a determination of the populations of more than four vibronic levels is meaningless. The reason is very simple and may be seen from Table VIII where the relative populations  $N_{av'}/N_{a0}$  (obtained for  $v'_{\max}=3$ ) are shown together with relative intensities of various  $a^3\Sigma_g^+, v' \rightarrow b^3\Sigma_u^+$  transitions in the spectral range under the study ( $\lambda = 230 - 400$  nm)

$$\xi_{v'} = \frac{\int_{\lambda_1}^{\lambda_2} N_{av'} \cdot A_b^{av'}(\lambda) d\lambda}{\int_{\lambda_1}^{\lambda_2} I_{ab}(\lambda) d\lambda}. \quad (18)$$

From the data in Table VIII it becomes clear that only 4% of the detected emission quanta originate from levels with  $v' > 3$ . The populations  $N_{av'}$  observed in the pure hydrogen capillary-arc discharge are quite close to those calculated in the framework of our simple model with  $T_{\text{vib}} \rightarrow 0$ .

To illustrate the correspondence between experimental and calculated relative continuum intensities we present data of our calculations on Fig. 5. The intensity calculated by Eq. (14) (the case of  $T_{\text{vib}} \rightarrow 0$ ) gives practically the same quality of the experimental data as that calculated by Eq. (1) with values of the  $N_{av'}$  from Table VIII in the wavelength range under the study. Below the short-wavelength margin differences appear between the calculations made with  $v'_{\text{max}} = 3$  (curve 2) and  $v'_{\text{max}} = 6$  (curve 3).

Furthermore, the first five Q-branch lines of Fulcher- $\alpha$  diagonal bands ( $d^3\Pi_u^- \rightarrow a^3\Sigma_g^+$  with  $v'=0-5$ ,  $N'=1-5$ ) were used to obtain the vibrational and gas temperatures for various discharge currents  $I$  by means of the method described above with a system of Eqs. (9) and (10) (see also [24,28]). The results are presented in Fig. 6. Note that our values of the gas temperature are in excellent agreement with those measured in [44] plotted also in Fig. 6. One may see a certain growth of both  $T_{\text{vib}}$  and  $T$  with an increase of the discharge current caused by a corresponding increase of the electron density and power input. Fulcher- $\alpha$  band intensities show a remarkable difference between  $T_{\text{vib}}$  and  $T$  analogous to that observed by CARS in [45]. On the other hand we tried to use the nomogram of Fig. 2 for a determination of the vibrational temperature. We plotted the experimental ratios  $J'_{ab}(\lambda, \lambda_0, T_{\text{vib}})$  on that figure as well. The experimental uncertainties of the ratio are too big. We can only estimate the upper limit of  $T_{\text{vib}} < 3000$  K. Moreover, there were no observable changes of the shape of the dissociation continuum within the range of the discharge current under the study. Taking into account the rather strong assumptions made in our excitation model we have to say that both spectroscopic methods are in fair agreement.

### C. Microwave discharge in $\text{H}_2+\text{Ar}$ mixture

The spectral intensity distribution of the continuum in the  $\text{H}_2+\text{Ar}$  microwave discharge has a noticeably different shape compared to that in pure hydrogen. Moreover, the shape was found to depend on the ratio of the components in the mixture ( $[\text{Ar}]:[\text{H}_2]$ ), which was changed from (19:1) to (1:4) under the same total pressure and power input. As an illustration some typical results are shown in Fig. 7. Here only the both limit cases of the (4:1) and (1:4) mixture are given. Note that measurements in between exhibit a monotonic dependence of the increased emission in the wavelength range around 300 nm. An analysis of various possible explanations of the observed phenomenon lead us to the assumption that an excitation transfer from excited Ar atoms to the hydrogen molecules might take place.

#### 1. $\text{Ar}^* \rightarrow \text{H}_2$ excitation transfer

Excitation transfer in collisions of metastable ( ${}^3\text{P}_{0,2}^o$ ) and resonant ( ${}^3\text{P}_1^o$  and  ${}^1\text{P}_1^o$ ) Ar I atoms with hydrogen molecules is known since the pioneer work of Lyman [46] and was investigated so far in plasma and beam experiments mainly as: 1) quenching of excited Ar and 2) additional excitation of VUV Lyman and Werner bands ( $B^1\Sigma_u^+, C^1\Pi_u \rightarrow X^1\Sigma_g^+$ )

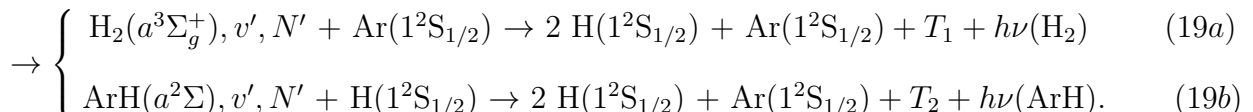
of  $\text{H}_2$ . The first attempts to study the role of this effect in the emission of the hydrogen dissociation continuum in  $\text{H}_2+\text{Ar}$  plasmas appeared quite recently [22,47–49].

The intensities of atomic hydrogen Balmer lines, Q-branch lines of Fulcher- $\alpha$  diagonal bands ( $d^3\Pi_u^- \rightarrow a^3\Sigma_g^+$ ) and the continuum in the wavelength range  $\lambda = 200 - 400$  nm have been measured in the active phase and in the afterglow of the hollow cathode discharge in pure hydrogen and its mixture with Ar (inner cathode diameter 6 mm, discharge currents 10 – 100 mA, total pressures about 1.5 mbar and Ar fraction in the mixture 20 – 80%) [47–49]. The experimental setup was almost the same as in [50].

It was observed that the increase of the Ar content in  $\text{H}_2+\text{Ar}$  mixture leads to: 1) an approximately linear growth of the total continuum intensity per  $\text{H}_2$  molecule; 2) a remarkable change in the shape of the spectral distribution of the continuum intensity [48]. The rectangular pulsed discharge mode was used for more or less independent variation on the gas temperature and for the measurement of the time-decay curves for the  $\text{H}_2$  continuum, (0-0) Q1, Q3 Fulcher- $\alpha$  lines of  $\text{H}_2$ , and Ar I ( $\lambda = 750.3$  nm) line. It was found that: (1) Within experimental errors the shape of the continuum is independent of the gas temperature in the range  $T = 300 - 800$  K. (2) In the pure hydrogen discharge the time-decay of atomic and molecular hydrogen emissions coincides with that of the discharge current (the rear edge about 5  $\mu\text{s}$ ). (3) The time-decay of Fulcher- $\alpha$  and Ar I lines in a  $\text{H}_2+\text{Ar}$  mixture is also in coincidence with the time behavior of the discharge current while the  $\text{H}_2$  continuum shows significantly slower exponential decay with a characteristic time depending on the ratio between the components in the mixture (about 15  $\mu\text{s}$ ) [47,49].

The last observation is a direct evidence for the existence of some additional (to the electron impact) excitation process leading to the continuum emission in the wavelength range under the study. The resulting spectral intensity distributions in  $\text{H}_2+\text{Ar}$  mixtures may be fitted (with  $\chi^2=0.8-1.2$ ) as a superposition of  $a^3\Sigma_g^+, v' \leftarrow X^1\Sigma_g^+, v=0$  electron impact excitation (of the  $v'=0-5$  vibronic levels) and additional excitation of the  $a^3\Sigma_g^+, v'=0$  vibronic level. The relative contribution of the last one is approximately proportional to the relative content of Ar in the  $\text{H}_2+\text{Ar}$  mixture [48,49].

An analysis of various possible mechanisms [49] shows that we have observed the excitation transfer from excited  $\text{Ar}^*$  atoms to the ground state  $\text{H}_2$  molecule. It may go through two different ways:



Here  $(\text{ArH}_2)^*$  denotes a temporary state of the system during the interaction,  $T_0$  and  $T_1, T_2$  are the initial and final kinetic energies of reacting particles in the mass center frame. The branching ratio between these two output channels of the reaction should depend on the initial excited state of the Ar atom and the vibro-rotational state of the molecule as well as on the collision energy  $T_0$ . As far as we know it is not established up to now in spite of a certain attempt in crossed beam experiments [4].

It may be shown, that if one wants to consider the excitation transfer possibility for  $1,3P_J^o$  argon atoms with various  $J$  values from the energy point of view, the existence of

vibro-rotational and translational energies of  $\text{H}_2$  molecules in plasma should be taken into account [49].

In our conditions the observed effects are most likely due to the collisions of the resonant  $^3\text{P}_1^\circ$  and metastable  $^3\text{P}_2^\circ$  argon atoms with the  $X^1\Sigma_g^+, v=0$  hydrogen molecules.

We measured the population densities of the Ar I  $3s^23p^54s$  ( $^3\text{P}_{0,1,2}^\circ$  and  $^1\text{P}_1^\circ$ ) levels by an ordinary self-absorption method with one mirror behind the discharge vessel [51].

Neglecting Stark broadening of the spectral lines the population of the initial state of  $k \leftarrow i$  absorption transition may be presented as

$$N_i = \sqrt{\frac{\pi}{4 \ln 2}} \frac{\Delta\nu_D}{f_0 f_{ik}} \kappa_0, \quad (20)$$

where

$$f_0 = \frac{\pi e^2}{m_e c} = 2.64 \cdot 10^{-2} \text{ cm}^2 \text{ s}^{-1}, \quad (21)$$

$f_{ik}$  – the oscillator strength for the  $k \leftarrow i$  transition in units of  $f_0$ ,  $\Delta\nu_D$  – the Doppler halfwidth depending on the gas temperature.

The absorption coefficient  $\kappa_0$  was obtained by numerical solutions of the following non-linear equation [51]:

$$2 \left[ 1 - \frac{S(2\kappa_0 l)}{S(\kappa_0 l)} \right] = \frac{(1+r) - I_m/I_0}{r}, \quad (22)$$

where  $I_m$  and  $I_0$  – the line intensities measured with and without the mirror,  $l$  – length of plasma column along the axis of observation,  $r$  – the reflection coefficient of the mirror and  $S(x)$  – the Ladenburgh-Lévy function calculated by formulas from [52].

The reflection coefficient has been determined experimentally by the measurement of several Ar I lines (603.1, 703.0, 714.7, 789.1, 860.6, 862.0, and 876.1 nm) which are free of self-absorption. It was found to be  $r = 0.52 \pm 0.02$  and independent on  $\lambda$ . We used the values of the oscillator strengths from [53].

The intensities of two or three different spectral lines were used for the population density determination of every  $3s^23p^54s$  level, namely:

$^3\text{P}_2^\circ$	—	763.511, 801.479, 811.531 nm
$^3\text{P}_1^\circ$	—	751.465, 738.398, 810.369 nm
$^3\text{P}_0^\circ$	—	794.815, 866.794 nm
$^1\text{P}_1^\circ$	—	826.452, 840.821 nm.

The conditions were the same as those in the measurements of the continuum intensity.

Typical results are shown in Fig. 8. The scaled populations are absolute values of the level population densities divided by their statistical weights  $(2J + 1)$ . They have the meaning of the average populations of the multiplet structure sublevels. In equilibrium conditions they should be almost equal to each other because the levels have almost the same energy – 11.55, 11.62, 11.72, and 11.83 eV for  $^3\text{P}_2^\circ$ ,  $^3\text{P}_1^\circ$ ,  $^3\text{P}_0^\circ$ , and  $^1\text{P}_1^\circ$ . One may see from Fig. 8 that in our conditions:

1. The populations of various sublevels of all resonant and metastable states coincide within the experimental errors. It is a direct manifestation of long effective lifetimes of the resonant levels (self-absorption of resonant emission) and a high enough rate of collisional transitions between the  $3s^23p^54s$  levels. So the metastable and resonant levels of Ar I are actually mixed in the plasma under the study.
2. The sublevel populations show a monotonic decreasing dependence on the total pressure which may be connected with: a decrease in the rate coefficient of electron impact excitation, an increase of collisional quenching and a possible decrease of microwave power applied to the plasma.
3. The total population of all 12 sublevels may reach  $10^{11} \text{ cm}^{-3}$  at low pressures. The rate coefficients of the  $\text{Ar}^* \rightarrow \text{H}_2$  excitation transfer are approximately  $10^{-10} \text{ cm}^3 \text{ s}^{-1}$  [16]. Thus the rate of the continuum excitation in the reaction is about  $10^{16} \text{ cm}^{-3} \text{ s}^{-1}$ . This is comparable with the observed total continuum emission (see Table IX) and should be taken into account together with direct electron impact excitation of the  $a^3\Sigma_g^+$  state of  $\text{H}_2$ .

Let us assume that the spectral distribution of the model continuum intensity may be presented as independent terms corresponding to three different excitation mechanisms:

$$I_{ab}^{\text{calc}}(\lambda) = A[c_1 I_{ab}(\lambda, 0) + c_2 I_b^{a0}(\lambda) + c_3 I_{\text{ArH}}(\lambda)], \quad (23)$$

where  $A$  – absolute scale normalization constant equal to total continuum intensity in the range of observation  $\lambda = 225 - 400 \text{ nm}$ ,  $I_{ab}(\lambda, 0)$  – spectral distribution of the continuum radiation caused by the electron impact excitation of  $\text{H}_2$  from lowest  $X^1\Sigma_g^+, v=0$  vibronic ground state [Eq. (14)],  $I_b^{a0}(\lambda)$  – the same due to the reaction (19a) for  $v'=0$  only,  $I_{\text{ArH}}(\lambda)$  – the spectral distribution corresponding to the reaction (19b) calculated in [4],  $c_i$  – the coefficients representing relative contributions of the components ( $\sum_i c_i = 1$ ). The spectral distributions  $I_{ab}(\lambda, 0)$ ,  $I_b^{a0}(\lambda)$  and  $I_{\text{ArH}}(\lambda)$  where normalized for unit area in the range of wavelengths  $\lambda = 225 - 400 \text{ nm}$ .

Then the spectral distributions of the continuum measured in the microwave plasma under various conditions were fitted by the function (23) according to Eq. (3). Typical results are presented in Table IX for five selected mixtures of Ar+H<sub>2</sub> from (1:4) up to (19:1). The first set of  $\chi^2$ -minimizations marked as ( $c_1, c_2, c_3 \neq 0$ ) is made without any additional conditions. One may see that the observed shape of the continuum may be described by three adjusted parameters of the expansion (23) with rather good precision ( $\chi^2 = 1 - 2$ ). Moreover the fittings show a negligible contribution of the reaction (19b), which cannot be considered as significant because the values of  $c_3$  are comparable with standard deviations of their determination. Figure 9 illustrates typical results of such a fitting. The contribution of the reaction (19b) is too small to be visible in the figure.

The second set of fittings was performed under the additional condition  $c_3 = 0$ . This version of the model provides almost the same precision in the description of the observed spectra taking into account only the first two mechanisms included into Eq. (23).

In contrast the third set of fittings was carried out for  $c_2 = 0$  thus neglecting a contribution of the reaction (19a). Again we got almost the same quality of fitting. These results are

the direct consequence of the similarity of spectral distributions of the continuum emission caused by the reactions (19a) for  $v'=0$  and (19b).

It should be noted, that *ab initio* potential curves of  $\text{ArH}^*$  were never checked experimentally and the spectral distribution of the  $\text{ArH}$  continuum was calculated in [4] in rough approximation of a harmonic oscillator. The precision of such calculations cannot be high nowadays. Taking this into account we may assume that the insignificant contribution of the reaction (19b) obtained in the first set of fittings is an accidental numerical result. Most probably it is without any physical meaning because two other sets [based on directly opposite assumptions about branching ratio between reactions (19a) and (19b)] gave us almost the same  $\chi^2$  values.

Therefore, we have to conclude that the precision and the wavelength range of our measurements together with the lack of dependable  $\text{ArH}^*$  transition probabilities do not allow us to distinguish contributions of the reactions (19a) and (19b). On the other hand, there is no doubt that in our conditions the role of the  $\text{Ar}^* \rightarrow \text{H}_2$  excitation transfer is well noticeable (10-30%).

## 2. Estimation of the rate of electron impact dissociation

As it was already mentioned in the introduction, the absolute value of the intensity of the continuum is directly connected with the rate of the radiative dissociation via spontaneous emission to the repulsive  $b^3\Sigma_u^+$  state. If absorption in the plasma volume may be neglected, then the rate of radiative dissociation due to  $a^3\Sigma_g^+ \rightarrow b^3\Sigma_u^+$  transitions is equal to the total continuum intensity (expressed in number of photons per  $\text{cm}^3$  in a second) integrated over the entire wavelength range

$$\left( \frac{d[\text{H}_2]}{dt} \right)_{ab} = \int_0^\infty I_{ab}(\lambda) d\lambda = \sum_{v'=0}^{v'_{\max}} \frac{N_{av'}}{\tau_{av'}}. \quad (24)$$

The wavelength range where we were able to measure the intensity was limited (see Fig. 4, 5, 7). So we detected only a part of the continuum emission. (Measurements in VUV are possible in principle, but they are not typical in most gas discharge and plasma technology applications due to their technical complexity and the difficulties in the sensitivity calibration and the spatial resolution.) The rest should be obtained by some extrapolation. In pure hydrogen discharge plasma the vibrational temperature is usually rather low and the Eqs. (1) and (12) may be used for the extrapolation. Two examples calculated with  $v'_{\max}=3$  and  $v'_{\max}=6$  are presented in Fig. 5 together with experimental data. One may see, that in our case: (1) The dependence of the total intensity (area under the curve) on the  $v'_{\max}$  is insignificant after  $v'_{\max}$  became high enough. (2) The contribution of the undetected part of the spectrum is rather significant (about 60% in the example).

The other, more general way of treating of spectroscopic data is a numerical solution of the reverse problem by  $\chi^2$ -minimization (3). The relative or absolute populations  $N_{av'}$  thus obtained may be used for the determination of the relative or absolute radiative dissociation rate. Radiative lifetimes are known, so an integration over wavelengths is not necessary and the procedure is reduced to only few summations in Eq. (24).

In low-pressure gas discharges the upper levels of the continuum transition are predominantly populated by  $a^3\Sigma_g^+ \leftarrow X^1\Sigma_g^+$  electron impact excitation. A dissociation of hydrogen molecules is also mainly caused by electron impact excitation of various intermediate excited electronic states, bound and repulsive ones. The relative contribution of various channels to the total electron impact dissociation cross section  $\sigma_{\text{diss}}(\varepsilon)$  was analyzed in [54], later supplemented with an application of the close-coupling calculations of the cross-sections [55]. It was found that singlet-triplet transitions play the major role,  $b^3\Sigma_u^+ \leftarrow X^1\Sigma_g^+$  and  $a^3\Sigma_g^+ \leftarrow X^1\Sigma_g^+$  being most prominent. The experimental data for  $\sigma_{\text{diss}}(\varepsilon)$  are available from [56].

All these cross-sections seem to have a rather similar shape as a function of the collision energy  $\varepsilon$ , except in the small region near the threshold, because an excitation of various electronic states obviously has different start-up energies. In [22] we proposed to use average values of ratios between the cross sections (determined far enough from threshold region) for the estimation of the rate of the radiationless  $b^3\Sigma_u^+ \leftarrow X^1\Sigma_g^+$  process  $(d[H_2]/dt)_{b \leftarrow X}$  and the total dissociation rate  $(d[H_2]/dt)_{\text{diss}}$  by multiplication of the measured total continuum intensity with certain coefficients, namely 4 and 15 correspondingly. Actually, the coefficients depend on the shape of the electron energy distribution function, for example, the total electron impact dissociation rate

$$\left( \frac{d[H_2]}{dt} \right)_{\text{diss}} = \frac{\alpha_{\text{diss}}}{\alpha_{a \leftarrow X}} \left( \frac{d[H_2]}{dt} \right)_{ab}. \quad (25)$$

Generally, the rate coefficients in (25) should be calculated with actual  $F(\varepsilon)$  by Eq. (7) [9,10]. If the distribution function is not available like in our present study, only rough estimations are possible. It is quite obvious that, when  $\varepsilon$ -dependences of the cross-sections have similar shapes, the ratio of the rate coefficients is less sensitive to the near-threshold region for  $F(\varepsilon)$  with a high content of fast enough electrons. To check the tendency we calculated the ratios for a Maxwellian distribution with an electron temperature of  $T_e = 1-10$  eV and the cross sections from [55,56]. The results are presented in Fig. 10. One may see that both ratios show sharp decrease for  $T_e < 5$  eV becoming almost independent from  $T_e$  for  $T_e > 5$  eV. It is quite typical for a low-pressure hydrogen discharge plasma to have a strongly non-Maxwellian  $F(\varepsilon)$  with a high density of fast electrons having energies sufficiently higher than the thresholds (see i.e. [57]). So we may use the asymptotics of Fig. 10 for the estimations. Numerical values of the coefficients are

$$\frac{\alpha_{b \leftarrow X}}{\alpha_{a \leftarrow X}} \sim 4.9 \quad \text{and} \quad \frac{\alpha_{\text{diss}}}{\alpha_{a \leftarrow X}} \sim 16. \quad (26)$$

In the pure hydrogen capillary-arc discharge we were not able to carry out absolute measurements because the plasma is inhomogeneous along the axis of observation and the effective length of the emitting plasma column is uncertain [57].

However, in the  $\text{H}_2 + \text{Ar}$  microwave plasma the length of emitting column ( $l \pm \Delta l$ ) is well defined and absolute continuum intensities were measured in a certain range of discharge conditions. But the Eqs. (24) and (26) are not valid any more, because  $\text{Ar}^* \rightarrow \text{H}_2$  excitation transfer plays an important role. The continuum intensity may be expressed as (23) and the total dissociation rate is a sum of the terms corresponding to the electron impact and the excitation transfer. It can be shown that in this case the total dissociation rate

$$\left( \frac{d[H_2]}{dt} \right)_{\text{total}} = \left( \frac{d[H_2]}{dt} \right)_{\text{diss}} + \left( \frac{d[H_2]}{dt} \right)_{\text{Ar}^*} \quad (27)$$

$$= A \left[ \frac{\alpha_{\text{diss}}}{\alpha_{a \leftarrow X}} c_1 \int_0^\infty I_{ab}(\lambda, 0) d\lambda + c_2 \int_0^\infty I_b^{a0}(\lambda) d\lambda + c_3 \int_0^\infty I_{\text{ArH}}(\lambda) d\lambda \right]. \quad (28)$$

Spectral distributions of the intensities in the second and third terms are mainly located in the wavelength range of our observations (about 90%). Only the first one, connected with  $a^3\Sigma_g^+, v' \leftarrow X^1\Sigma_g^+ v=0$  excitation needs the extrapolation described above. Therefore, the total dissociation rate in our conditions may be calculated from the measured continuum intensity. The results are shown in Fig. 11(a,b) for various pressures and ratios of the components in the mixture. They may be interpreted only qualitatively.

Figure 11(a) shows that the dissociation rate monotonically decreases with increasing pressure. This effect may have several reasons, for instance, increased collisional quenching of the excited molecules at higher pressures or diminished microwave power transfer to the molecules. Under constant total pressure an increase of the dissociation rate with growing  $H_2$  content in the mixture can be noticed in Fig. 11(b).

#### IV. CONCLUSION

Our attempt to study the informational contents of the intensity of the hydrogen dissociation continuum and to check its applicability for plasma diagnostics has been *a priori* limited in two different respects.

1) We intended to have an experimental technique as simple as possible and, in particular, to stay on the basis of emission spectroscopy only. Then the methods would be especially useful in various industrial applications including rather easy *in situ* control of plasma processing. The approach has in principle a backside because the knowledge of the actual electron energy distribution function and its spatial distribution may be of importance for a correct extraction of the information about plasma parameters. Langmuir probe measurements of electron energy distributions are not a problem nowadays [even in the cases of space-charge layers [57], RF [58,59] and microwave discharges (see [60] and Refs. herein)].

We limited ourselves with intensity measurements in the more or less easy detectable near-UV region because the following second restriction of our attempt seems to be more significant.

2) Our analysis of the known characteristics of radiative and collisional processes involved into the mechanism of formation of observable continuum emission led us to the conclusion that in spite of numerous efforts the situation is still unsatisfactory. Therefore, only simple models are available and justified. The corona-like model of the excitation (neglecting the rotational structure of upper vibronic levels) and the Franck-Condon approximation for electron impact excitation are actually available and justified right now.

Nevertheless, even in such complicated conditions we were happy to find that more or less accurate measurements of relative and absolute spectral distributions of the continuum intensity may be used for certain estimations of the vibrational temperature, for the analysis of the excitation mechanisms and for getting information about the rate of hydrogen dissociation by electron impact.

The last one looks most prospective because in some cases it may be already used as it is. If, for example, one is interested in the relative dependence of the electron impact dissociation rate on the position in plasma or on discharge conditions, the information may be easily obtained just by a measurement of the continuum emission intensity even without any calibrations. The method of the determination of the absolute rate of the electron impact dissociation may be considerably improved, if the electron energy distribution function would be determined experimentally or calculated somehow. Then there would be no need to use our graph in Fig. 10 but to calculate the values in an explicit way.

This rather easy and independent method of determination of the absolute values of the rate of electron impact dissociation of hydrogen may be used in gas discharge physics and in plasma chemistry within two approaches.

1) It may be used for the determination of the hydrogen dissociation degree (which is often considered as a very important plasma parameter), if one is able to determine the effective mean lifetime of atoms in plasma with certain theoretical model of diffusion and association of atoms (see e.g. [61]).

2) If the value of the dissociation degree is determined by one of the existing methods (see [62,63])) then the effective lifetime of atoms in plasma may be determined with the help of the rate of dissociation and the corresponding balance equation for atoms.

In both cases the method proposed in the present work is giving new opportunities.

Further improvements need more detailed information about the elementary processes especially those about the cross sections of electronic-vibrational (better electronic-vibro-rotational)  $a^3\Sigma_g^+, v', N' \leftarrow X^1\Sigma_g^+, v, N$  electron impact excitation and the rate coefficients of the quenching of  $a^3\Sigma_g^+, v', N'$  levels in collisions with electrons, atoms and molecules. We certainly understand those are not simple problems, but we may hope that the needs of plasma diagnostics and our present work may be considered as some kind of the challenge for our colleagues working in the field of electronic and atomic collision physics.

## ACKNOWLEDGMENTS

The authors are indebted to Prof. J. Conrads, S. N. Manida and Dr. M. Schmidt for general support of the project. This work was supported, in part, by the Deutsche Forschungsgemeinschaft, Sonderforschungsbereich 198, by the Russian Foundation for Support of Basic Research (grant No 95-03-09394a), and by the Program of Support of International Collaboration of Ministry of High Education of the Russian Federation. Dr. A. S. Melnikov is thankful to the Deutsche Forschungsgemeinschaft, Sonderforschungsbereich 198, who provided a scholarship for his training in Germany and to the INP-Greifswald for its hospitality. The authors are thankful to Prof. N. Sadeghi (Grenoble) for the discussion which stimulated the second and the third fittings presented in Table IX. One of us (BPL) is thankful to Prof. V. N. Ostrovsky (SPbSU) who informed him about work [40]. The authors thank Mr. D. Gött for skillful technical assistance.

## REFERENCES

- [1] H. M. James and A. S. Coolidge, *Phys. Rev.* **55**, 184 (1939).
- [2] R. G. Fowler and T. M. Holzberlein, *J. Chem. Phys.* **42**, 3723 (1965).
- [3] R. T. Thompson and R. G. Fowler, *J. Quant. Spectrosc. Radiat. Transfer* **12**, 117 (1972).
- [4] C. R. Lishawa, J. W. Feldstrin, T. N. Stewart, and E. E. Muschlitz, *J. Chem. Phys.* **83**, 133 (1985).
- [5] T. L. Kwok, S. Guberman, A. Dalgarno, and A. Posen, *Phys. Rev. A* **34**, 1962 (1986).
- [6] B. P. Lavrov, A. V. Loginov, and V. P. Prosikhin, *Appl. VINITI N7897-V88*, 19 (1988), 04.11.1988.
- [7] B. P. Lavrov, A. V. Loginov, and V. P. Prosikhin, *Opt. Spectrosc.* **67**, 1220 (1989).
- [8] A. N. Zaidel and E. Shreider, *Vacuum Ultraviolet Spectroscopy* (Ann Arbor-Humphrey Science Publishers, Moscow, 1967).
- [9] B. P. Lavrov and V. P. Prosikhin, *Opt. Spectrosc.* **58**, 317 (1985).
- [10] B. P. Lavrov and V. P. Prosikhin, *Opt. Spectrosc.* **64**, 498 (1988).
- [11] R. O. Doyle, *J. Quant. Spectr. Radiat. Transfer* **8**, 1555 (1968).
- [12] W. H. Smith and R. Chevalier, *Astrophys. J.* **177**, 835 (1972).
- [13] F. G. Houtermans, *Helv. Phys. Acta* **33**, 933 (1960).
- [14] A. Cohn and M. Marcucci, *J. Appl. Phys.* **44**, 1930 (1973).
- [15] L. I. Gudzenko and C. I. Yakovlenko, *Plasmennye Lasery (Plasma Lasers in Russian)* (Atomisdat, Moscow, 1978), p. 253.
- [16] J. Godart and V. Puech, *Chem. Phys.* **46**, 23 (1980).
- [17] J. Bretagne, J. Godart, and V. Puech, *J. Phys. B* **14**, 761 (1981).
- [18] V. S. Greben'kov and L. P. Shishatskaya, *Sov. J. Opt. Technol.* **10**, 33 (1979).
- [19] B. P. Lavrov and L. P. Shishatskaya, *Sov. J. Opt. Technol.* **46**, 692 (1979).
- [20] V. S. Greben'kov, B. P. Lavrov, and M. V. Tyutchev, *Sov. J. Opt. Technol.* **49**, 115 (1982).
- [21] B. P. Lavrov and M. V. Tyutchev, *Sov. J. Opt. Technol.* **53**, 612 (1986).
- [22] M. Käning *et al.*, in *Book of Papers of Frontiers in Low Temperature Plasma Diagnostics II* (Arbeitsgemeinschaft Plasmaphysik, Bochum, 1997), pp. 197–200.
- [23] D. J. Hudson, *Statistics, Lectures on Elementary Statistics and Probability* (Geneva, 1964).
- [24] B. P. Lavrov, in *Plasma Chemistry (in Russian)*, edited by B. M. Smirnov (Energoatomizdat, Moscow, 1984), Chap. Electronic-Rotational Spectra of Diatomic Molecules and Diagnostics of Non-Equilibrium Plasma, pp. 45–92.
- [25] R. Bleekrode, *IEEE J. Quantum Electronics* **EQ-5**, 27 (1969).
- [26] B. P. Lavrov and J. K. Otorbaev, *Opt. Spectrosc.* **45**, 859 (1978).
- [27] B. P. Lavrov, *Opt. Spectrosc.* **48**, 375 (1980).
- [28] S. A. Astashkevich *et al.*, *J. Quant. Spectrosc. Radiat. Transfer* **56**, 725 (1996).
- [29] M. L. Burshtein *et al.*, *Opt. Spectrosc.* **68**, 166 (1990).
- [30] B. P. Lavrov and L. L. Pozdeev, *Opt. Spectrosc.* **66**, 479 (1989).
- [31] B. P. Lavrov, *Spectroscopy and Kinetics of Electronical-Vibro-Rotational Excitations of Diatomic Molecules in Gas Discharge Plasmas*, Dr. Sc. thesis, 1988.
- [32] R. E. Imhof and F. H. Read, *J. Phys. B* **4**, 1063 (1971).
- [33] G. C. King, F. H. Read, and R. E. Imhof, *J. Phys. B* **8**, 665 (1975).

- [34] K. A. Mohamed and G. C. King, *J. Phys. B* **12**, 2809 (1979).
- [35] G. R. Möhlmann and F. J. De Heer, *Chem. Phys. Lett.* **43**, 240 (1976).
- [36] P. Baltayan and O. Nedelec, *J. Quant. Spectrosc. Radiat. Transfer* **16**, 207 (1976).
- [37] B. P. Lavrov, V. N. Ostrovsky, and V. I. Ustimov, *J. Phys. B* **14**, 4701 (1981).
- [38] B. P. Lavrov, A. S. Melnikov, L. L. Pozdeev, and N. V. Tokarev, *Appl. VINITI N5634-V90*, 28 (1990), 21.06.1990.
- [39] A. I. Dratchev, B. P. Lavrov, and V. P. Prosikhin, *Appl. VINITI N491-V86*, 40 (1986), 23.01.1986.
- [40] M. T. Lee, L. E. Machado, L. M. Brescansin, and G. D. Meneses, *J. Phys. B* **24**, 509 (1991).
- [41] A. I. Drachev and B. P. Lavrov, *High Temp. (USSR)* **26**, 129 (1988).
- [42] A. Ohl, in *Microwave Discharges: Fundamentals and Applications*, Vol. Physics 302 of *NATO ASI Series, B*, edited by C. M. Ferreira and M. Moisan (Plenum Press, New York, 1993), pp. 205–214.
- [43] V. I. Malyshev, *Introduction in Experimental Spectroscopy (in Russian)* (Nauka, Moscow, 1979), p. 478.
- [44] B. P. Lavrov and M. V. Tyutchev, *Sov. J. Opt. Technol.* **49**, 741 (1982).
- [45] *Nonequilibrium vibrational kinetics*, edited by M. Capitelli (Springer-Verlag, Berlin, 1986).
- [46] T. Lyman, *Astrophys. J.* **33**, 98 (1911).
- [47] A. S. Melnikov, Ph.D. thesis, St. Petersburg State University, 1996.
- [48] B. P. Lavrov, A. S. Melnikov, and M. A. Tchaplyguine, in *Abstracts of 29<sup>th</sup> European Group for Atomic Spectroscopy*, edited by H. Kronfeld (European Physical Society, Berlin, Germany, 1997), Vol. 21C, pp. 574–575.
- [49] B. P. Lavrov and A. S. Melnikov, *Opt. Spectrosc.* (to be published) .
- [50] B. P. Lavrov and A. S. Melnikov, *Opt. Spectrosc.* **75**, 676 (1993).
- [51] *Spectroscopy of Gas Discharge Plasmas (in Russian)*, edited by S. E. Frisch (Nauka, Leningrad, 1970).
- [52] S. E. Frisch, *Optical Atomic Spectra (in Russian)* (Phis. Mat. Gis., Leningrad, 1963).
- [53] A. A. Radzig and B. M. Smirnov, *Reference Data on Atoms, Molecules and Ions*, Vol. 31 of *Springer Series in Chemical Physics* (Springer, Berlin, 1988).
- [54] S. Chung, C. C. Lin, and E. T. R. Lee, *Phys. Rev. A* **12**, 1340 (1975).
- [55] S. Chung and C. C. Lin, *Phys. Rev. A* **17**, 1874 (1978).
- [56] S. J. B. Corrigan, *J. Chem. Phys.* **43**, 4381 (1965).
- [57] N. V. Bublina, B. P. Lavrov, and V. P. Prosikhin, *Sov. Phys. Tech. Phys.* **32**, 1228 (1987).
- [58] V. A. Godyak, R. B. Piejak, and B. M. Alexandrovich, *Plasma Sources Sci. Technol.* **1**, 36 (1992).
- [59] U. Flender *et al.*, *Plasma Sources Sci. Technol.* **5**, 61 (1996).
- [60] U. Kortshagen, A. Shivarova, E. Tatarova, and D. Zamfirov, *J. Phys. D: Appl. Phys.* **27**, 301 (1994).
- [61] B. P. Lavrov and V. J. Simonov, *High Temp. (USSR)* **25**, 649 (1987).
- [62] B. P. Lavrov, *Opt. Spectrosc.* **42**, 250 (1977).
- [63] V. Schulz-von der Gathen and H. F. Döbele, *Plasma Chemistry and Plasma Processing* **16**, 461 (1995).

## FIGURES

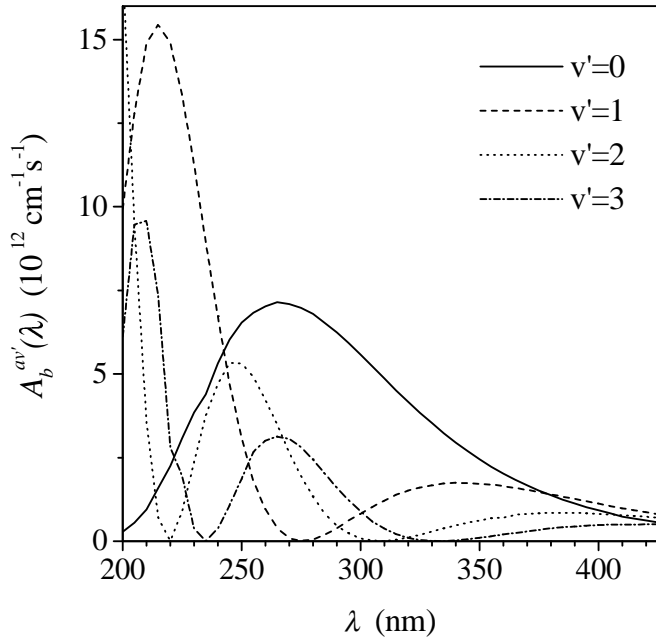


FIG. 1. Spectral distribution of  $a^3\Sigma_g^+, v' \rightarrow b^3\Sigma_u^+$  spontaneous emission probability for various initial vibronic levels of the H<sub>2</sub> molecule [6,7].

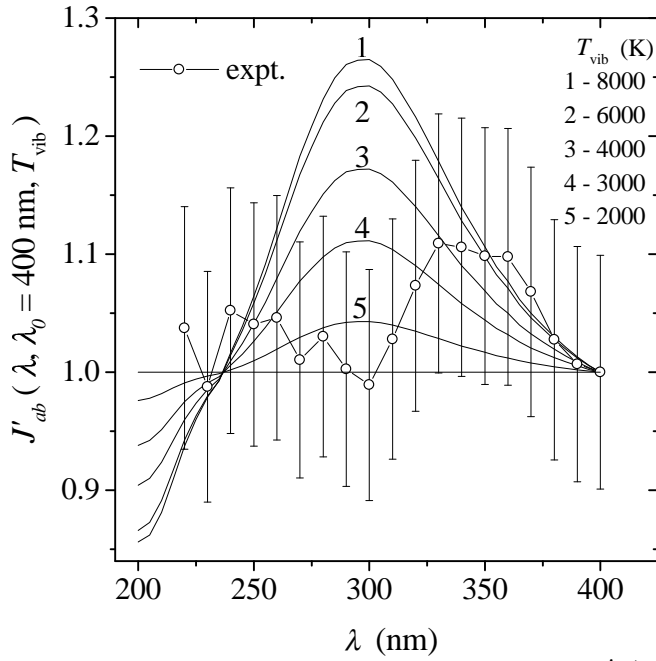


FIG. 2. Normalized continuum emission  $J'_{ab}(\lambda, \lambda_0=400 \text{ nm}, T_{\text{vib}})$  for various vibrational temperatures  $T_{\text{vib}}$  from 2000 to 8000 K. Experimental data ( $\circ$ ) from capillary-arc discharge with  $I=100$  mA.

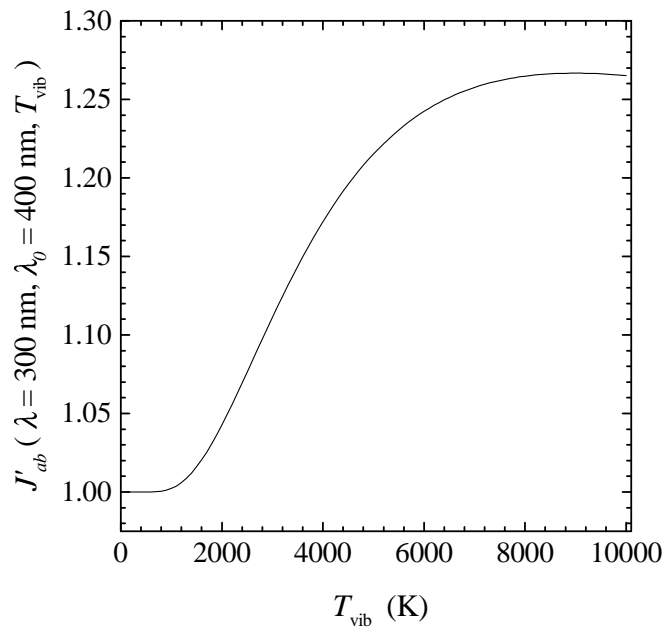


FIG. 3. Normalized continuum emission  $J'_{ab}(\lambda, \lambda_0=400 \text{ nm}, T_{\text{vib}})$  at  $\lambda=300 \text{ nm}$ .

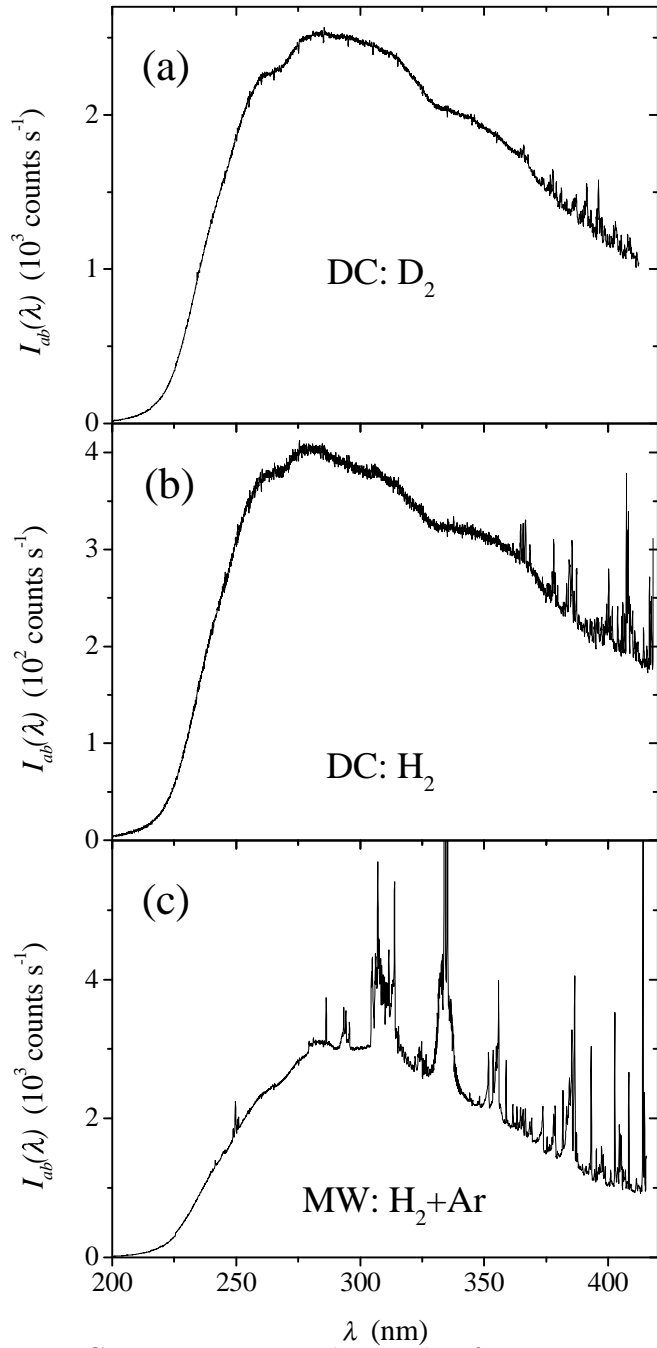


FIG. 4. Experimental records of continuum measured in DC capillary-arc discharges in  $D_2$  and  $H_2$  ( $I=100$  mA) and in the microwave discharge ( $p=0.5$  mbar,  $H_2:Ar=1:1$ ), here spectral distribution of sensitivity is not taken into account.

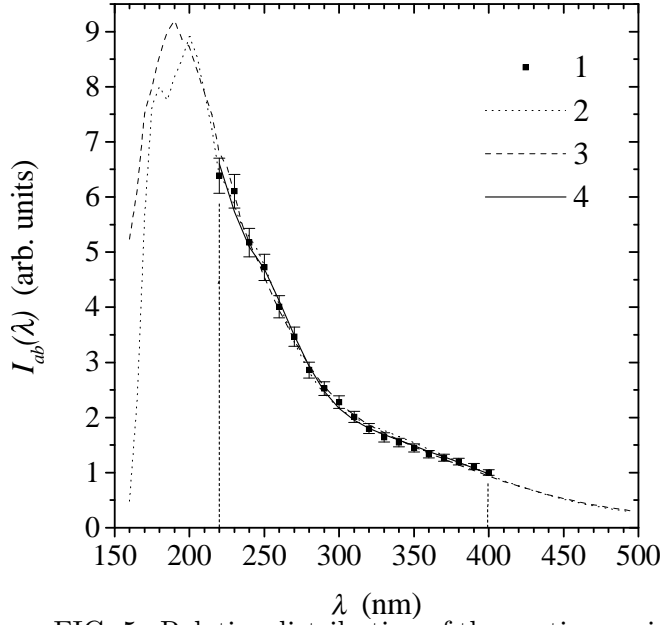


FIG. 5. Relative distribution of the continuum intensity measured in the capillary-arc discharge with  $I=100$  mA (data points 1) and those calculated for  $T_{\text{vib}} \rightarrow 0$  by Eqs. (1) and (3) with  $v'_{\text{max}}=3$  (curve 2) and  $v'_{\text{max}}=6$  (curve 3) and fitting of experimental data points 1 (curve 4).

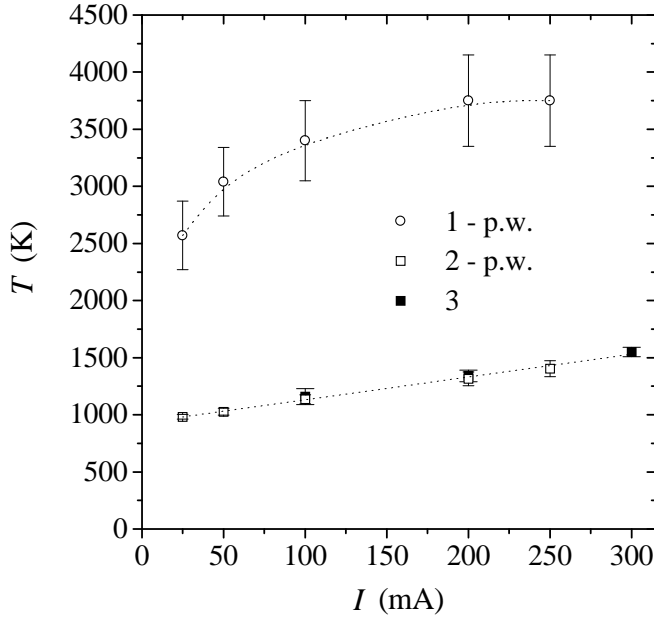


FIG. 6. Vibrational (1) and rotational (2, 3) temperatures in the ground  $X^1\Sigma_g^+$  state of the  $\text{H}_2$  determined from the emission of Fulcher- $\alpha$  bands in the capillary-arc pure hydrogen plasma for various discharge currents. The data (1, 2) – present work, (3) – Ref. [44].

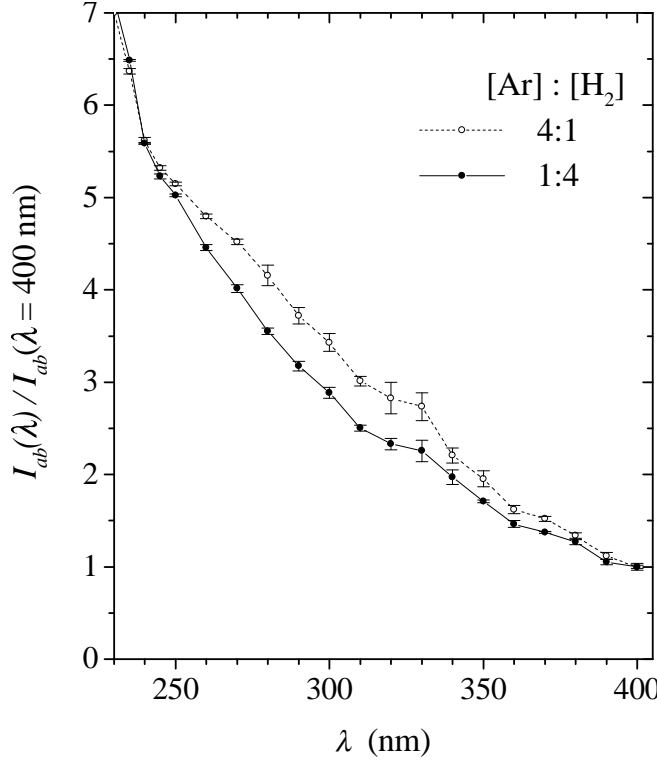


FIG. 7. The relative continuum intensity (normalized for unity at  $\lambda = 400$  nm) measured in a  $\text{H}_2+\text{Ar}$  microwave plasma for two different ratios of the components at  $p = 0.5$  mbar.

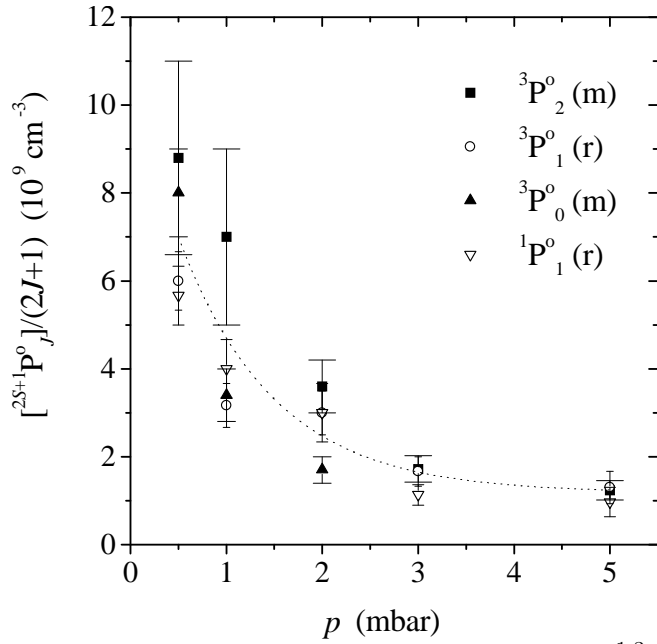


FIG. 8. The scaled population densities of  ${}^1,3\text{P}_J^o$  levels of Ar I as a function of total pressure  $p$  for constant gas mixture  $\text{H}_2+\text{Ar}$  (1:1) in the microwave discharge plasma. The total average population of all  $3s^23p^54s$  levels may be obtained by multiplication of 12 to the dashed curve.

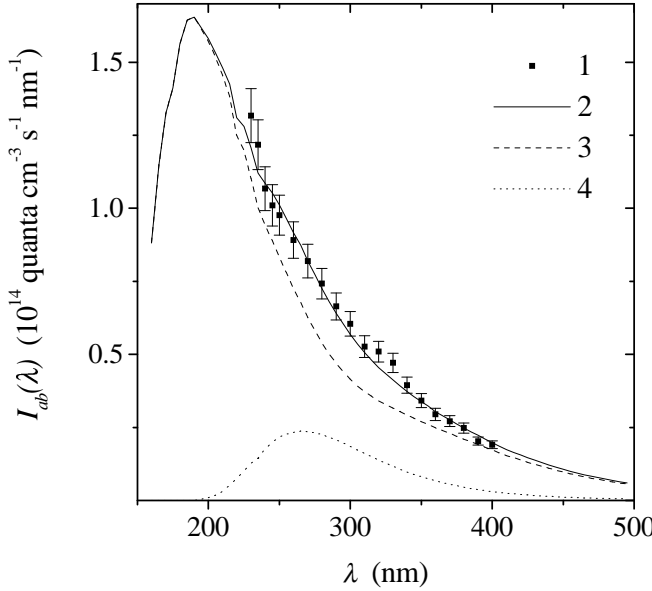


FIG. 9. Spectral density of the continuum emission in the  $\text{H}_2+\text{Ar}$  (1:1) microwave plasma for total pressure  $p = 0.5$  mbar. 1 – experimental data points, 2 – calculated by Eqs. (3) and (23) with the optimal set of parameters  $A, c_1, c_2, c_3$  shown in Table IX, 3 – the contribution of the electron impact excitation for  $T_{\text{vib}} \rightarrow 0$  K with  $v'_{\text{max}}=3$ , 4 – contribution of the excitation transfer to  $a^3\Sigma_g^+, v'=0$ .

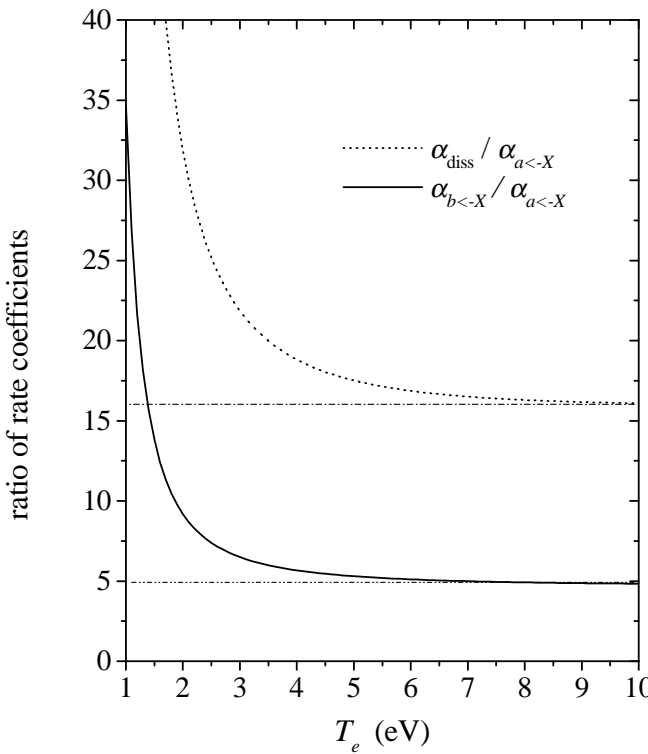


FIG. 10. Ratios of the rate coefficients of electron impact excitation of  $b^3\Sigma_u^+$  ( $\alpha_{b\leftarrow X}$ ),  $a^3\Sigma_g^+$  ( $\alpha_{a\leftarrow X}$ ) states and of the electron impact dissociation ( $\alpha_{\text{diss}}$ ) calculated as a function of the electron temperature.

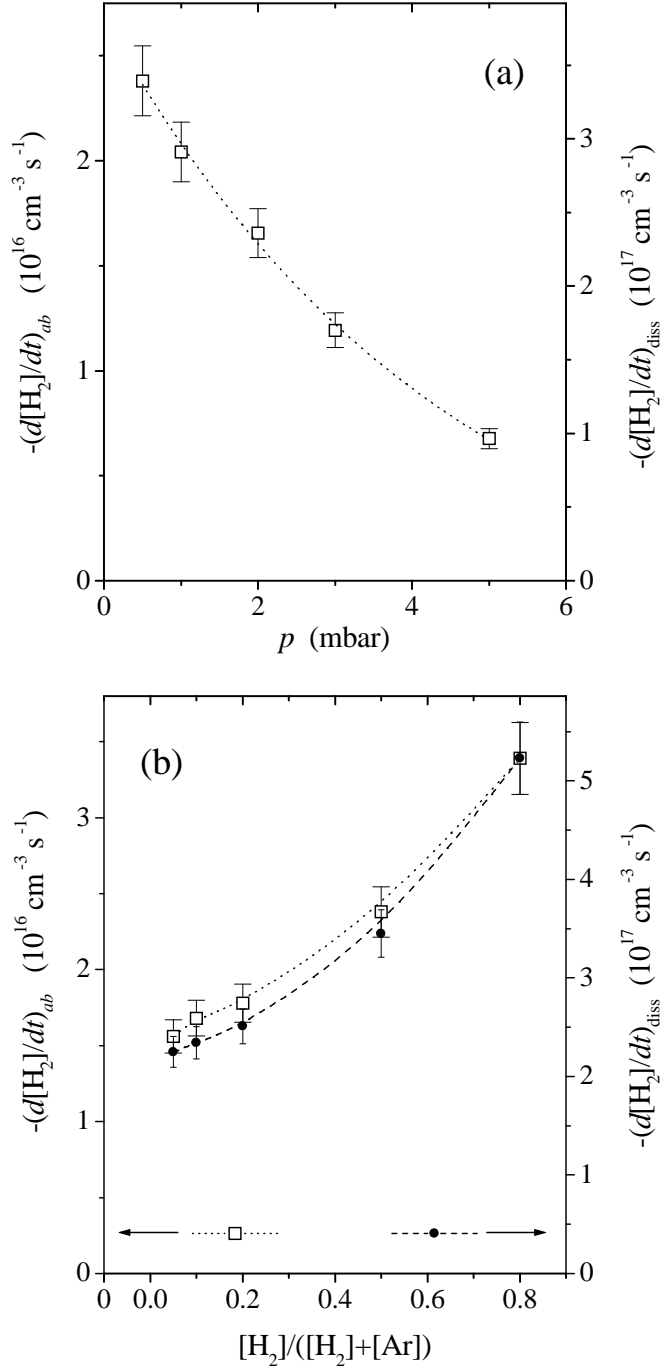


FIG. 11. Radiative dissociation rate  $-(d[\text{H}_2]/dt)_{ab}$  ( $\square$ ) and estimated total electron impact dissociation rate  $-(d[\text{H}_2]/dt)_{\text{diss}}$  ( $\bullet$ ) obtained for the  $\text{H}_2$  + Ar microwave discharge: (a) as a function of the total pressure  $p$  for constant gas mixture (1:1) and (b) for various gas mixtures under constant total pressure  $p = 0.5$  mbar.

## TABLES

 TABLE I. Spectral distributions of transition probability for  $a^3\Sigma_g^+, v'=0-6 \rightarrow b^3\Sigma_u^+$  spontaneous emission of the H<sub>2</sub> molecule (Refs. [6,7])

$\lambda$ [nm]	$A_b^{av'}(\lambda) (10^{12} \text{ cm}^{-1} \text{ s}^{-1})$							$J_{ab}(\lambda, \lambda_0, 0),$ $\lambda_0 = 400 \text{ nm}$
	$v'=0$	1	2	3	4	5	$v'=6$	
160	0	0	0	3.220	49.674	3.795	22.997	5.570
170	0	0	1.714	34.647	9.474	23.008	14.436	8.005
180	0	0.395	16.152	24.766	11.127	0.144	2.297	9.116
190	0	3.701	26.715	0.231	10.235	10.524	5.725	9.798
200	0.283	9.938	17.191	6.123	0.047	2.873	5.463	9.290
210	0.949	14.879	3.565	9.571	4.340	0.697	0.077	8.388
220	2.252	14.894	0.016	2.799	6.257	4.182	1.898	7.233
230	3.851	11.283	2.370	0.377	3.070	4.066	3.662	6.451
240	5.315	6.723	4.702	0.386	0.386	1.681	2.498	5.513
250	6.540	3.087	5.315	1.871	0.164	0.135	0.704	4.845
260	7.025	0.948	4.222	3.010	1.154	0.165	0.025	4.195
270	7.090	0.085	2.645	3.056	1.971	0.851	0.262	3.617
280	6.792	0.049	1.330	2.440	2.176	1.416	0.797	3.135
290	6.249	0.389	0.463	1.598	1.918	1.609	1.161	2.731
300	5.582	0.819	0.079	0.893	1.414	1.456	1.256	2.420
310	4.867	1.224	0	0.367	0.869	1.126	1.118	2.174
320	4.165	1.509	0.108	0.101	0.471	0.755	0.866	1.984
330	3.530	1.671	0.295	0.006	0.197	0.451	0.597	1.832
340	2.946	1.748	0.474	0.020	0.045	0.226	0.372	1.695
350	2.453	1.717	0.618	0.100	0.005	0.080	0.193	1.564
360	2.021	1.647	0.695	0.202	0.011	0.018	0.083	1.434
370	1.667	1.530	0.818	0.296	0.058	0.002	0.024	1.329
380	1.373	1.399	0.846	0.379	0.117	0.016	0.004	1.216
390	1.125	1.265	0.844	0.445	0.179	0.047	0.007	1.107
400	0.921	1.127	0.818	0.486	0.228	0.088	0.026	1
410	0.735	0.985	0.781	0.499	0.271	0.127	0.051	0.890
420	0.621	0.865	0.729	0.504	0.303	0.161	0.080	0.804
430	0.514	0.752	0.674	0.497	0.320	0.190	0.104	0.718
440	0.423	0.654	0.615	0.477	0.327	0.207	0.127	0.639
450	0.343	0.567	0.559	0.455	0.327	0.221	0.144	0.566
460	0.283	0.488	0.503	0.429	0.322	0.226	0.157	0.501
470	0.241	0.420	0.452	0.397	0.310	0.229	0.164	0.444
480	0.203	0.363	0.402	0.366	0.297	0.229	0.168	0.394
490	0.169	0.312	0.359	0.337	0.281	0.221	0.168	0.347

TABLE II. Radiative lifetimes of  $d^3\Pi_u^-, v, N=1$  levels and spontaneous emission transition probabilities of  $d^3\Pi_u^-, v, N=1 \rightarrow a^3\Sigma_g^+, v, N=1$  spectral lines of H<sub>2</sub>, calc. - semiempirical calculation in adiabatic approximation.

$v$	$\tau_{dv1}$ (ns)		$A_{av1}^{dv1}$ ( $\mu\text{s}^{-1}$ )
	expt. <sup>a</sup>	calc. <sup>b</sup>	
0	$40.7 \pm 1.4$	$38.7 \pm 2.0$	$24.4 \pm 1.4$
1	$38.4 \pm 1.3$	$39.7 \pm 2.1$	$20.6 \pm 1.1$
2	$39.5 \pm 1.9$	$40.9 \pm 2.2$	$16.9 \pm 1.0$
3	$39.5 \pm 0.9$	$42.2 \pm 2.2$	$13.6 \pm 0.8$
4	$19.0 \pm 1.0$	$43.6 \pm 2.4$	$10.6 \pm 0.6$
5	$15.2 \pm 1.2$	$45.5 \pm 2.5$	$8.1 \pm 0.5$
6	$16.0 \pm 3.0$	—	$5.9 \pm 0.4$

<sup>a</sup>Refs. [28,29]

<sup>b</sup>Ref. [10]

<sup>c</sup>Ref. [30]

TABLE III. Experimental and *ab initio* data on the radiative lifetimes of  $a^3\Sigma_g^+, v'$  levels of H<sub>2</sub>, p. w. - present work, values calculated from data in Ref. [38].

$v'=0$	$\tau_{av'}$ (ns)						Ref.
	1	2	3	4	5	$v'=6$	
theory							
11.9	11.0	10.1	9.7	—	—	—	[1]
11.6	10.2	9.17	8.40	7.81	7.30	6.90	[5]
12.4	11.5	10.3	9.29 <sup>a</sup>	8.64 <sup>a</sup>	8.07 <sup>a</sup>	7.63 <sup>a</sup>	p. w.
experiment							
..... 35±8 <sup>b</sup> .....							
11.0 ± 0.42	10.6 ± 0.6	—	—	—	—	—	[2]
26 ± 2	—	—	—	—	—	—	[3]
11.9 ± 1.2	10.8 ± 1.1	..... 10±2 <sup>b</sup> .....	—	—	—	—	[12]
..... 10.45±0.25 <sup>b</sup> .....							
9.94 ± 0.39	9.1 ± 1.0	—	—	—	—	—	[33]
..... 9.62±0.20 <sup>b</sup> .....							
..... — .....							

<sup>a</sup>These values were extrapolated on the basis of the data from Ref. [5] (for details see text).

<sup>b</sup>Values were obtained as some average of numerous vibrational levels marked by dotted line.

TABLE IV. Relative cross sections for electron impact excitation (in the maximum) of the  $d^3\Pi_u^-, v'$  levels from  $X^1\Sigma_g^+, v=0$  level and corresponding ratios of Franck-Condon factors.

$v'$	$\sigma_{X01}^{dv'1}/\sigma_{X01}^{d21}$					FCF
	[35]	[36]	[37]	[9]	present work	
0	0.57	0.68	$0.52 \pm 0.07$	$0.66 \pm 0.07$	$0.70 \pm 0.07$	0.55
1	0.86	1.09	$0.91 \pm 0.13$	$0.88 \pm 0.09$	$0.96 \pm 0.09$	0.95
2	1.00	1.00	$1.00 \pm 0.14$	$1.00 \pm 0.10$	$1.00 \pm 0.10$	1.00
3	0.78	0.86	$0.96 \pm 0.14$	$0.77 \pm 0.08$	$0.84 \pm 0.08$	0.86
4	—	—	—	$0.35 \pm 0.04$	$0.87 \pm 0.09^a$	0.66
5	—	—	—	$0.19 \pm 0.02$	$0.60 \pm 0.06^a$	0.47
6	—	—	—	$0.11 \pm 0.01$	$0.32 \pm 0.03^a$	0.33

<sup>a</sup>Cross sections for  $v'=4-6$  recalculated from data in Ref. [9] (for details see text).

TABLE V. Franck-Condon factors for  $a^3\Sigma_g^+, v' \leftarrow X^1\Sigma_g^+, v$  transitions of H<sub>2</sub> [38].

$v'$	$Q_{Xv0}^{av'0}$						
	$v=0$	1	2	3	4	5	$v=6$
0	0.20761	0.39958	0.28411	0.09341	0.01439	0.00089	0.00001
1	0.25478	0.06483	0.08307	0.32592	0.21741	0.05018	0.00378
2	0.20249	0.00503	0.16438	0.00281	0.20634	0.30686	0.10324
3	0.13470	0.06063	0.05177	0.08235	0.07231	0.07873	0.34105
4	0.08235	0.09580	0.00050	0.10148	0.00727	0.12529	0.01180
5	0.04840	0.09603	0.01522	0.04193	0.06678	0.00933	0.11680
6	0.02803	0.07908	0.04137	0.00439	0.07005	0.01583	0.04615

TABLE VI. Franck-Condon factors for  $d^3\Pi_u^-, v' \leftarrow X^1\Sigma_g^+, v$  transitions of H<sub>2</sub> [38].

$v'$	$Q_{Xv0}^{dv'0}$						
	$v=0$	1	2	3	4	5	$v=6$
0	0.09995	0.29272	0.33797	0.19710	0.06160	0.00994	0.00070
1	0.17029	0.16255	0.00036	0.16128	0.29619	0.16752	0.03860
2	0.18029	0.02851	0.08310	0.10636	0.00914	0.23640	0.26345
3	0.15451	0.00075	0.10888	0.00041	0.12133	0.02528	0.11911
4	0.11833	0.02432	0.05755	0.03636	0.05553	0.04245	0.09099
5	0.08505	0.05077	0.01334	0.06851	0.00096	0.08332	0.00043
6	0.05899	0.06393	0.00002	0.05697	0.01538	0.03661	0.04690

TABLE VII. Results of  $\chi^2$ -minimisation of the experimental data shown on Fig. 5 with various number of adjusted parameters ( $v'_{\max}+1$ ).

$v'_{\max}$	$\chi^2$	$\rho_{\max}$	$\left(\frac{\Delta N_{av'}}{N_{av'}}\right)_{\max}$
0	57.1	$10^{-8}$	0.093
1	9.89	0.62	0.108
2	2.10	0.73	0.124
3	0.426	0.84	0.127
4	0.308	0.98	0.833
5	0.149	1.00	6.670
6	0.159	1.00	2.820

TABLE VIII. Experimental and calculated relative population densities for  $T_{\text{vib}} \rightarrow 0$  of the  $a^3\Sigma_g^+, v'$  vibronic states and relative intensities  $\xi_{v'}$  in the range  $\lambda=230\text{-}400$  nm. Pure hydrogen capillary-arc discharge  $I=100$  mA - see Fig. 5. Errors in brackets correspond to last digit(s).

$v'$	$N_{av'}/N_{a0}$		$\xi_{v'}$	
	expt.	calc.	expt.	calc.
0	1.00(3)	1.00	0.50(2)	0.50
1	1.20(4)	1.14	0.27(1)	0.25
2	0.79(7)	0.81	0.14(1)	0.14
3	0.86(11)	0.52	0.09(1)	0.06
4	—	0.28	—	0.03
5	—	0.15	—	0.01
6	—	0.08	—	0.01

TABLE IX. Results of estimation of the dissociation rate in the microwave plasma with constant pressure  $p = 0.5$  mbar for various  $\text{H}_2+\text{Ar}$  mixtures. Table sections for certain parameter combinations in Eq. (28). Errors in brackets correspond to last digit.

[Ar]:[H <sub>2</sub> ]	electron impact $T_{\text{vib}} \rightarrow 0$	additional channels		$\chi^2$	$-(d[\text{H}_2]/dt)_{ab}$ (10 <sup>16</sup> cm <sup>-3</sup> s <sup>-1</sup> )	
		(19a)	(19b)		(1) <sup>a</sup>	(2) <sup>b</sup>
$c_1, c_2, c_3 \neq 0$						
1:4	0.90(4)	0.10(6)	0.00(3)	0.93	1.40	3.4
1:1	0.79(4)	0.21(6)	0.00(3)	1.04	1.05	2.4
4:1	0.74(5)	0.23(7)	0.03(3)	1.27	0.81	1.8
9:1	0.72(5)	0.25(7)	0.03(4)	1.66	0.78	1.7
19:1	0.77(6)	0.18(8)	0.05(4)	1.90	0.70	1.6
$c_1, c_2 \neq 0; c_3 = 0$						
1:4	0.90(4)	0.10(4)	—	0.89	1.37	3.3
1:1	0.79(4)	0.21(4)	—	0.98	1.05	2.4
4:1	0.73(5)	0.27(5)	—	1.26	0.82	1.8
9:1	0.71(5)	0.29(5)	—	1.64	0.78	1.7
19:1	0.75(6)	0.25(6)	—	1.96	0.70	1.6
$c_1, c_3 \neq 0; c_2 = 0$						
1:4	0.97(3)	—	0.03(2)	1.09	1.36	3.4
1:1	0.93(3)	—	0.07(3)	1.68	1.06	2.6
4:1	0.90(4)	—	0.10(3)	2.10	0.82	2.0
9:1	0.89(4)	—	0.11(3)	2.58	0.79	1.9
19:1	0.90(4)	—	0.10(3)	2.35	0.71	1.7

<sup>a</sup>For  $\lambda = 225 - 400$  nm.

<sup>b</sup>Extrapolated for all  $\lambda$ .